A New Metric for Automated Stability Identification in Time Domain Milling Simulation

Andrew Honeycutt
Department of Mechanical Engineering
and Engineering Science,
University of North Carolina at Charlotte,
9201 University City Boulevard,
Charlotte, NC 28223
e-mail: ahoney15@uncc.edu

Tony L. Schmitz[1]
Department of Mechanical Engineering
and Engineering Science,
University of North Carolina at Charlotte,
9201 University City Boulevard,
Charlotte, NC 28223
e-mail: tony.schmitz@uncc.edu

A new metric is presented to automatically establish the stability limit for time domain milling simulation signals. It is based on periodically sampled data. Because stable cuts exhibit forced vibration, the sampled points repeat over time. Periodically sampled points for unstable cuts, on the other hand, do not repeat with each tooth passage. The metric leverages this difference to define a numerical value of nominally zero for a stable cut and a value greater than zero for an unstable cut. The metric is described and is applied to numerical and experimental results.
[DOI: 10.1115/1.4032586]

Keywords: milling, stability, Poincaré section, time domain simulation

Introduction

Machining dynamics has received significant attention in the literature because: (1) it is industrially relevant; and (2) it poses a challenging modeling opportunity due to the required solution of the second-order delay differential equations that are used to describe the system behavior. In particular, the prediction of stable and unstable (chatter) cutting conditions based on the selected operating parameters, typically spindle speed and chip width, has been investigated by many authors using time domain, analytical, and semi-analytical techniques.

The purpose of this study is to establish a metric that automatically differentiates between stable and unstable behavior for the time domain simulation of milling processes. The approach is based on periodic sampling of milling signals and follows from the use of Poincaré maps to study state space orbits in nonlinear dynamics. The paper is organized as follows. First, background information on milling stability prediction is provided. Second, the application of periodic sampling and Poincaré maps to results from a new efficient time domain milling simulation is demonstrated. Third, the new stability metric is presented. Fourth, experimental results are compared to simulation. Finally, conclusions are presented.

Background

In science and engineering fields, new insights are typically followed by a burst of follow-on research activity and corresponding publications. These insights tend to serve as a catalyst to the research community and often result in new discoveries, improved understanding of fundamental phenomena, and enhanced modeling capabilities. For machining, one such period of rapid progress began in the mid-19th century [1]. During this time, self-excited vibrations were first described using time-delay differential equations [2]. The notion of "regeneration of waviness" was promoted as the feedback mechanism (time-delay term), where the previously cut surface combined with the instantaneous vibration state dictates the current chip thickness, force level, and corresponding vibration response [3–6]. This work resulted in analytical algorithms that were used to produce the now well-known stability lobe diagram that separates the spindle speed-chip width domain into regions of stable and unstable behavior [5–17].

In 1998, a similar step forward in the understanding of machining behavior was initiated. Davies et al. used once-per-revolution sampling to characterize the synchronicity of cutting tool motions (measured using a pair of orthogonal capacitance probes) with the tool rotation in milling [18]. They observed the traditional quasi-periodic chatter associated with the secondary (subcritical) Hopf, or Neimark-Sacker, bifurcation[2] that can occur for systems described by periodic time-delay differential equations [19]. However, they also recorded period-3 tool motion (i.e., motion that repeated with a period of three cutter revolutions) during partial radial immersion milling. They noted that this behavior was "inconsistent with existing theory" [18]. In 2000, Davies et al. further examined the stability of highly interrupted machining [20]. They developed a two-stage map to describe: (1) noncutting motions governed by an analytical solution; and (2) motions during cutting using an approximation (fixed tool position with a change in momentum). They reported a doubling of the number of optimally stable spindle speeds when the time in cut is small. Milling experiments confirmed the new, low radial immersion best speeds.

In 2001, Moon and Kalmár-Nagy reviewed the "prediction of complex, unsteady, and chaotic dynamics" in machining [19]. They listed the various contributors to nonlinear behavior, including the loss of tool-workpiece contact due to large amplitude vibration and workpiece material constitutive relations, and highlighted previous applications of nonlinear dynamics methods to the study of chatter [21–26]. They also specified the use of phase-space methods, such as Poincaré maps, to identify changes in machining process dynamics.

Time domain simulation is a powerful tool for exploring milling behavior [27,28]. For example, Zhao and Balachandran implemented time domain simulation, which incorporated loss of tool-workpiece contact and regeneration, to study milling [29]. They identified secondary Hopf bifurcation and suggested that "period-doubling bifurcations are believed to occur" for low radial immersions [29]. They included bifurcation diagrams for limited axial depth of cut ranges at two spindle speeds to demonstrate the two bifurcation types.

Davies et al. extended their initial work in 2002 to present the first analytical stability boundary for highly interrupted machining [30]. It was based on modeling the cutting process as a kicked harmonic oscillator with a time delay and followed the two-stage map concept described previously [20].They used the frequency content of a microphone signal to establish the existence of both secondary Hopf and period-2 (or period-doubling or flip) instabilities. Mann et al. also provided experimental validation of secondary Hopf and period-2 instabilities for up and down milling [31]. They reported "a kind of period triple phenomenon" [31] observed using the once-per-revolution sampled displacement signal recorded from a single degree-of-freedom flexure-based machining platform.

The semidiscretization, time finite element analysis, and multi-frequency methods were also developed to produce milling

[1]Corresponding author.
Manuscript received August 24, 2015; final manuscript received January 4, 2016; published online March 8, 2016. Assoc. Editor: Laine Mears.

[2]A bifurcation is a dramatic change in the system state, or behavior.

stability charts that demonstrate both instabilities [32–36]. In Ref. [37], it was shown using the semidiscretization method that the period-2 bifurcation exhibits closed, lenslike, curves within the secondary Hopf lobes, except for the highest speed stability lobe. Simultaneous quasi-periodic (secondary Hopf) and period-2 bifurcation behavior was also observed. It was reported that this "combination" behavior occurred at unstable axial depths of cut above the period-2 lobes. Additionally, period-3 instability was seen and it was noted that this "periodic chatter" with period-3 (or higher) always occurred above a secondary Hopf stability limit. The same group [38] reported further experimental evidence of quasi-periodic (secondary Hopf), period-2, -3, -4, and combined quasi-periodic and period-2 chatter, depending on the spindle speed-axial depth values for a two degrees-of-freedom dynamic system. A perturbation analysis was performed in Ref. [39] to identify the secondary Hopf and period-2 instabilities. Additionally, numerical integration was implemented to construct a bifurcation diagram for a selected spindle speed that demonstrated the transition from stable operation to quasi-periodic chatter as the axial depth is increased. Stépán et al. continued to explore the nonlinear aspects of milling behavior in 2005 [40]. They described stable period-2 motion where the tool does not contact the workpiece in each tooth period (even in the absence of runout). For a two flute cutter, for example, only one tooth contacts the workpiece per revolution; they referred to this condition as the "fly over effect" and included a bifurcation diagram for these proposed stable and unstable period-2 oscillations.

The effect of the helix angle on period-2 instability was first studied by Zatarain et al. [41]. They found that, depending on the helix angle, the closed, lenslike, curves within the secondary Hopf lobes change their size and shape. They also found that these closed islands of stability can appear even in the highest speed stability lobe (in contrast to the results when helix angle is not considered). Experimental results were provided. This work was continued in Ref. [42], where the authors emphasized that at axial depths equal to the axial pitch of the cutter teeth, the equation of motion becomes an autonomous delay differential equation so the period two instability is not possible. Patel et al. studied the helix effect in up and down milling using the time finite element approach [43].

Time Domain Simulation, Periodic Sampling, and Poincaré Maps

The forcing function in milling is defined by the periodic entry and exit of each tooth on the rotating cutter to/from the workpiece material. This periodic forcing function occurs at the tooth passing frequency (i.e., the product of the spindle speed and number of teeth) and excites the tool and/or workpiece dynamics. The time delay is introduced because the surface left by the previous tooth affects the chip thickness for the current tooth. Time domain simulation includes the numerical solution of the time delay, second-order differential equations of motion, but is generally considered computationally expensive relative to analytical or semi-analytical stability prediction techniques [44].

To reduce execution time, a new "predefinition" approach is applied here. In this technique, the cutter angles and nominal chip thickness values at each time step are described outside the time-marching simulation loop. The approach is described here and summarized in Fig. 1.

- Determine the cutter rotation angle, d, in each time step, dt, by dividing the spindle speed, Ω, by dt.
- Calculate the number of steps, S, per one tooth period (e.g., $\pi/2$ rad rotation for a cutter with four teeth) using d and the number of teeth, N_t, i.e., $S = 2\pi/N_t \cdot d$.
- Define a vector, θ, of increasing tooth angles in step size d for a single tooth.
- Copy this vector N_t times into a single vector, ϕ, that describes all tooth angles for one revolution of the cutter.
- Determine the cut entry/exit angles based on the radial depth and up or down milling conditions.
- Calculate the chip thickness vector for a single tooth using $f_t \sin\theta$, where f_t is the feed per tooth. If the tooth angle is not bounded by these angles, the chip thickness entry is set to zero.
- Copy this vector N_t times into a single vector, h, that describes the angle-dependent nominal chip thickness values for one revolution of the cutter.
- Specify the number of cutter revolutions, R, for the simulation.
- Copy the ϕ and h vectors R times into two vectors, ϕ_{sim} and h_{sim}, that define the cutter angles and nominal chip thickness values for the entire simulation.

After these two vectors are predefined, the simulation is completed using the following steps within a single loop with index i, which is completed $S \cdot N_t \cdot R$ times (once for each time step over the selected number of revolutions).

- If the current entry in $h_{\text{sim}}(i)$ is greater than zero, calculate the current vibration normal to the cut surface, $n(i) = x(i-1)\sin_{\text{sim}}(i) - y(i-1)\cos_{\text{sim}}(i)$, where i is the loop index, and x/y are the cutter deflections from the previous time step. Using $n(i)$, calculate the instantaneous chip thickness, $h(i) = h_{\text{sim}}(i) + n(i-S) - n(i)$, which depends on the normal vibration for both the current (i) and previous ($i-S$) teeth.
- If $h(i)$ is greater than zero, calculate the tangential and normal cutting force components using $F_t = k_{tc}bh(i) + k_{te}b$ and $F_n = k_{nc}bh(i) + k_{ne}b$, where b is the axial depth of cut, and the k terms are the cutting force coefficients (the c subscripts denote cutting and the e subscripts represent edge, or rubbing, terms). Project these forces into the x and y directions via $F_x(i) = F_t\cos_{\text{sim}}(i) + F_n\sin_{\text{sim}}(i)$ and $F_y(i) = F_t\sin_{\text{sim}}(i) - F_n\cos_{\text{sim}}(i)$. See Fig. 2.
- If $h(i)$ is less than or equal to zero, set the x and y forces to zero. Note that this step incorporates the nonlinearity that occurs when the vibration levels are large enough that a tooth leaves the cut (in this case, the chip thickness is negative).
- Given the current x and y forces, calculate the current acceleration in the x and y directions: $\ddot{x}(i) = [F_x(i) - c_x\dot{x}(i-1) - k_x x(i-1)]/m_x$ and $\ddot{y}(i) = [F_y(i) - c_y\dot{y}(i-1)$

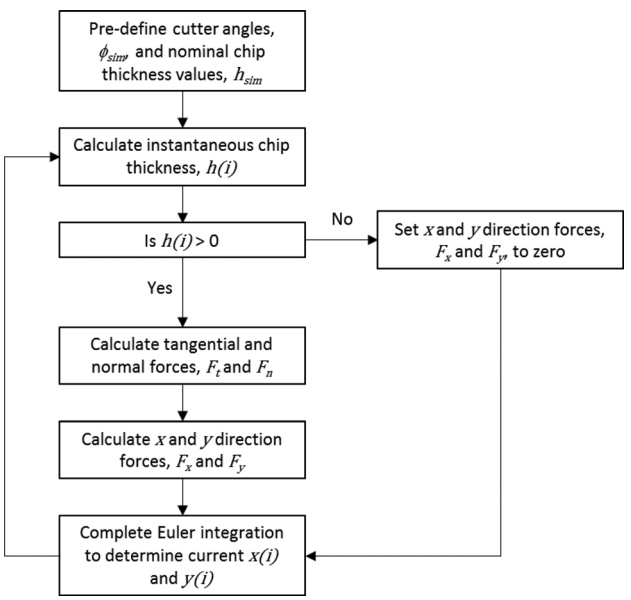

Fig. 1 Flow diagram for the time domain simulation

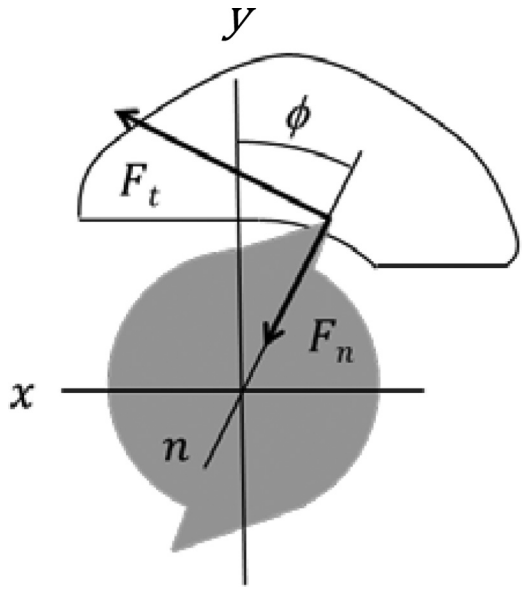

Fig. 2 Cutting force geometry. The normal and tangential direction cutting forces, F_n and F_t, are identified. The fixed *x* and *y* directions, as well as the rotating normal direction, *n*, are also shown. The angle ϕ defines the tooth angle. The tool feed is to the right for the clockwise tool rotation, and the axial depth is in the *z* direction.

$-k_y y(i-1)]/m_y$, where $m_{x/y}$, $c_{x/y}$, and $k_{x/y}$ are the modal mass, viscous damping, and stiffness values for the tool. Also, the single overdot identifies velocities.

- The current velocities are calculated using Euler integration: $\dot{x}(i) = \dot{x}(i-1) + \ddot{x}(i) \cdot dt$ and $\dot{y}(i) = \dot{y}(i-1) + \ddot{y}(i) \cdot dt$. This fixed-step numerical integration scheme was selected because it is robust provided the time step is sufficiently small. Other solution strategies can alternately be applied.
- The current displacements are calculated by: $x(i) = x(i-1) + \dot{x}(i) \cdot dt$ and $y(i) = y(i-1) + \dot{y}(i) \cdot dt$.

This simple description can be extended to include:

(1) helix angle—the axial depth of cut is segmented into multiple slices with width db, where each slice is rotated relative to the next by the angle $db \cdot \tan/r$, which depends on the helix angle, γ, and the tool radius, r
(2) multiple tool modes—the x and y forces are used to calculate the acceleration, velocity, and displacement for each tool mode (represented by the modal parameters), and the results are summed in each direction
(3) flexible workpiece—the x and y forces are also used to determine the workpiece deflections, again by numerical integration, and the relative tool-workpiece vibration is used to calculate the instantaneous chip thickness
(4) runout of the cutter teeth—the chip thickness is updated by the runout of the current tooth
(5) unequal teeth spacing—the tooth angle vector is modified to account for the actual tooth pitch.

A powerful interrogation tool for milling dynamics is the Poincaré map, where the tool (or workpiece) displacement is plotted versus the velocity and then sampled once per tooth period. This sampling establishes the synchronicity of the motion (response) with the cutting force (excitation). For stable cutting conditions, only forced vibration is present, and the sampled point repeats for each tooth passage. For unstable cutting, on the other hand, the repetition of a single point is not observed, and the character of the sampled points identifies the type of instability: secondary Hopf or period-n bifurcations.

As an example, consider symmetric, single degree-of-freedom dynamics for 5% radial immersion up milling with a spindle speed of 30,000 rpm. The modal parameters are: 721 Hz natural frequency, 0.009 viscous damping ratio, and 4.1×10^5 N/m stiffness. The cutter has one tooth, a 45 deg helix angle, and an 8 mm diameter. The aluminum alloy cutting force coefficients are: $k_{tc} = 604 \times 10^6$ N/m^2 and $k_{nc} = 223 \times 10^6$ N/m^2 (zero edge coefficients). The time-dependent x vibration, as well as the once-per-tooth sampled points, for a stable cut (0.5 mm axial depth), is displayed in Fig. 3. The corresponding Poincaré map is also shown; the sampled points repeat with each tooth period for the forced vibration response. Figure 4 shows the results for a period-2 bifurcation (2.5 mm); here, two clusters of points occur. Figure 5 represents a secondary Hopf bifurcation (5 mm); an elliptical grouping of points is seen in the Poincaré map for the quasi-periodic response.

This transition in behavior with increasing axial depth (30,000 rpm spindle speed) is conveniently presented using a bifurcation diagram, where the sampled displacement points from the Poincaré maps (e.g., Figs. 3–5) are plotted versus the control variable, which is axial depth of cut in this case. In the diagram, a stable cut appears as a single point (i.e., the repeating sampled points) for the selected axial depth. A period-2 bifurcation appears as a pair of points offset from each other in the vertical direction. An example diagram is provided in Fig. 6, where the stable depths up to 0.77 mm (labeled A, representing Fig. 3), as well as the period-2 from 0.77 mm to 2.59 mm (B, Fig. 4) and secondary Hopf (C, Fig. 5) bifurcation depths, are observed. The bifurcation

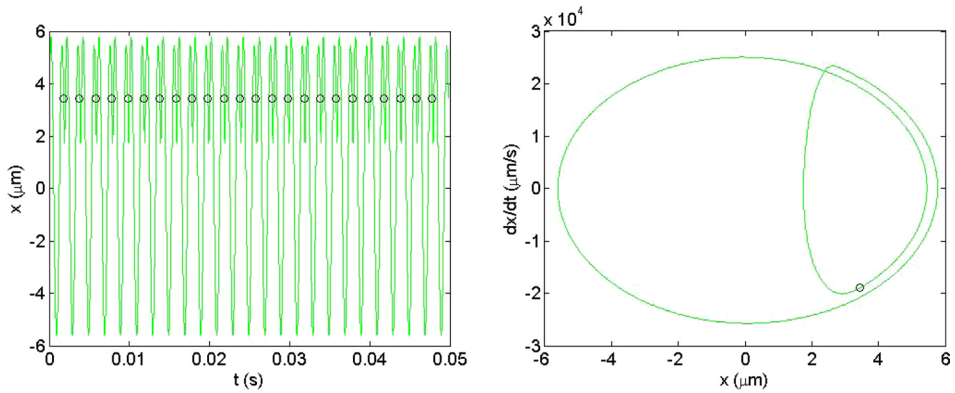

Fig. 3 Stable cut, $b = 0.5$ mm (left) time response for *x* (feed) direction displacement; (right) Poincaré map which plots *x* displacement versus velocity. The once-per-tooth sampled points are displayed as circles.

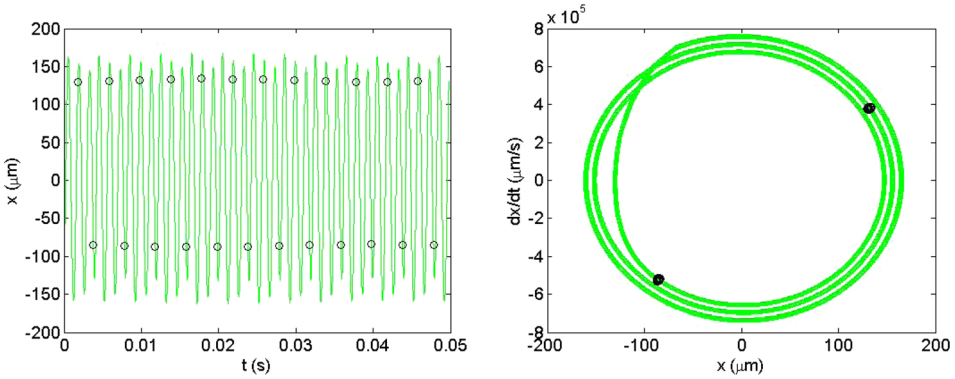

Fig. 4 Period-2, $b = 2.5$ mm (left) time response for x (feed) direction displacement; (right) Poincaré map

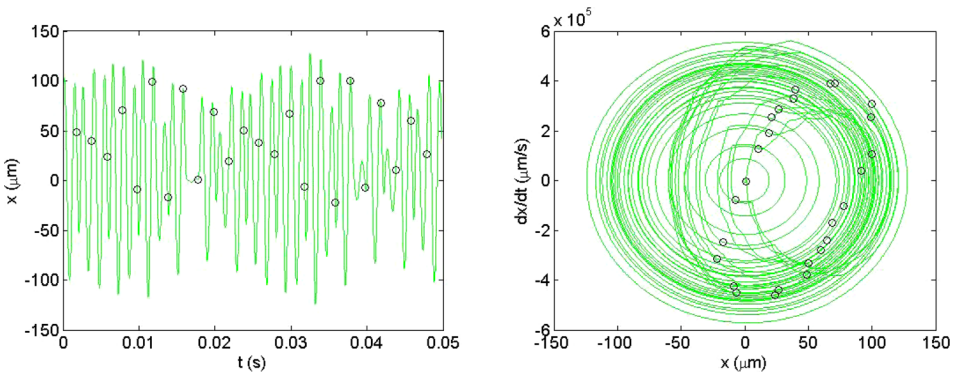

Fig. 5 Secondary Hopf, $b = 5.0$ mm (left) time response; (right) Poincaré map

diagram also reveals a combination of period-2 and secondary Hopf instabilities (D) and period-7 bifurcation (E).

Stability Metric

While bifurcation diagrams (e.g., Fig. 6) provide an effective visual representation of the stability behavior using the once-per-tooth sampled data, it is also beneficial to represent the process stability over a large domain of spindle speeds (in addition to axial depths). This is the traditional stability lobe diagram. To construct this stability map, time domain simulations are completed over the desired grid of spindle speed and axial depth values. A primary challenge for time domain simulation, however, is automatically establishing the stability limit. In this research, a new stability criterion based on the once-per-tooth sampled data is implemented. The metric builds on the approach in Refs. [45–47] where the standard deviation of the periodically sampled milling audio signal was calculated.

The new stability metric is $M = \sum_{i=2}^{N} |x_s(i) - x_s(i-1)|/N$, where x_s is the vector of once-per-tooth sampled x displacements, and N is the length of the x_s vector. Other variables, such as y displacement or cutting force could be selected as well. With this new stability metric, the absolute value of the differences in successive sampled points is summed and then normalized. As seen in Fig. 3, the sampled points repeat for a stable cut, so the M value is ideally zero. For unstable cuts, however, $M > 0$.

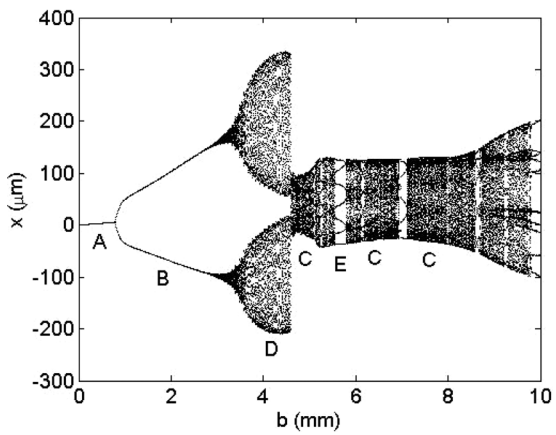

Fig. 6 Bifurcation diagram for selected spindle speed (30,000 rpm) and system dynamics

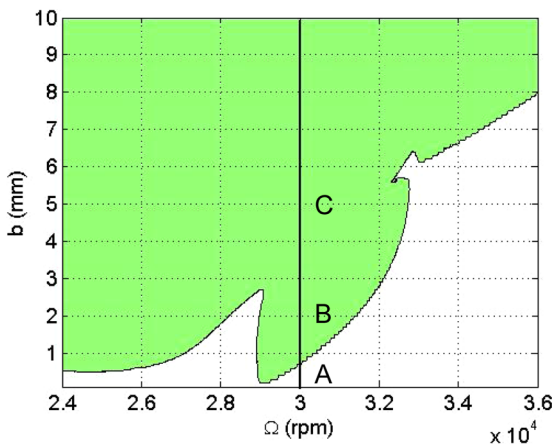

Fig. 7 Simulated stability map ($M = 1$ μm contour)

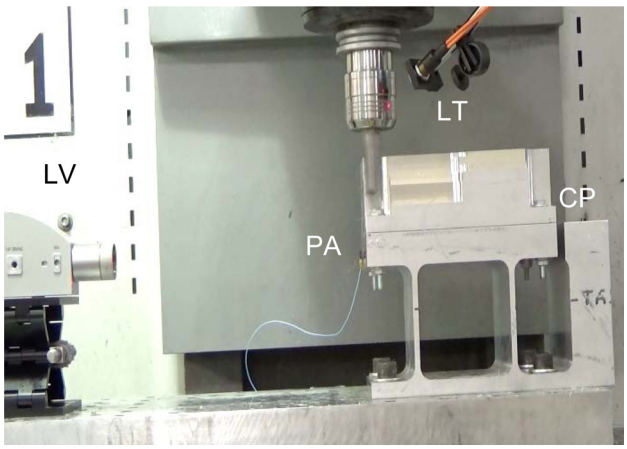

Fig. 8 Milling experimental setup with laser vibrometer (LV), piezo-accelerometer (PA), laser tachometer (LT), and capacitance probe (CP)

For the milling system defined previously, an example stability map is provided in Fig. 7, where the spindle speed resolution is 10 rpm, the axial depth resolution is 0.1 mm, and the initial transients (i.e., the homogeneous part of the differential equation solution) were removed prior to analysis. Figure 7 is a height map of M values, where only one contour line is plotted. This contour represents an M value of 1 μm and identifies the stability limit as a function of spindle speed and axial depth ($M = 0$ was not used due to limited numerical precision; instead, the small value of 1 μm was selected). Figure 7 includes a vertical line at 30,000 rpm. This is the range of axial depths used to generate the bifurcation diagram in Fig. 6. It is seen that stable behavior is achieved up to 0.77 mm (A). There is then a transition to the period-2 bifurcation (B); this is the elliptical-shaped zone immediately above the stability limit in the 29,000–33,000 rpm range. At higher axial depths, there is a transition to secondary Hopf instability (C). The stability diagram does not provide the amplitude and bifurcation behavior, however. In this way, the bifurcation diagram can be considered to be a data-rich vertical slice of the stability lobe diagram.

Experimental Results

Stability testing was completed to validate the time domain simulation using the flexure-based setup displayed in Fig. 8. The setup included a parallelogram leaf-type flexure with an aluminum workpiece mounted on top. The in-process vibration data were collected using a laser vibrometer (velocity) and capacitance probe (displacement). Once-per-tooth sampling was accomplished using a laser tachometer. Acceleration was also measured using a piezoelectric accelerometer. The flexure dynamics were identified by modal testing: 163 Hz natural frequency, 0.011 viscous damping ratio, and 5.2×10^6 N/m stiffness in the flexible (feed) direction. The dynamics for the 19.1 mm diameter tool (one tooth) were symmetric: 1050 Hz natural frequency, 0.045 viscous damping ratio, and 3.85×10^7 N/m stiffness. The aluminum alloy cutting force coefficients were: $k_{tc} = 792 \times 10^6$ N/m^2, $k_{nc} = 392 \times 10^6$ N/m^2, $k_{te} = 26 \times 10^3$ N/m, and $k_{ne} = 28 \times 10^3$ N/m.

A bifurcation diagram for a spindle speed of 3800 rpm and radial depth of 5 mm (26% radial immersion up milling, 0.15 mm feed per tooth) was predicted by simulation, and then cuts were performed from 1 mm to 7 mm axial depths in 0.5 mm steps. The capacitance probe displacement signal was sampled using the laser tachometer to construct an experimental bifurcation diagram; Fig. 9 provides the comparison between prediction and experiment. For this axial depth of cut range, period-3 bifurcations were observed. Figure 10 shows the simulated and experimental

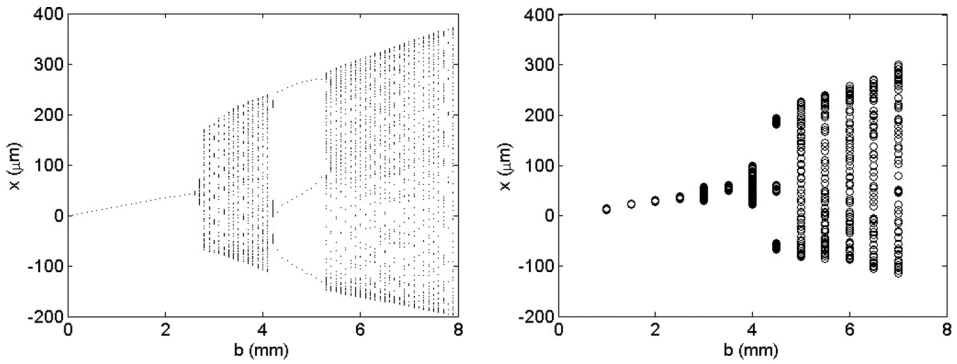

Fig. 9 Bifurcation diagram for 3800 rpm, 26% radial immersion (left) simulated; (right) experiment

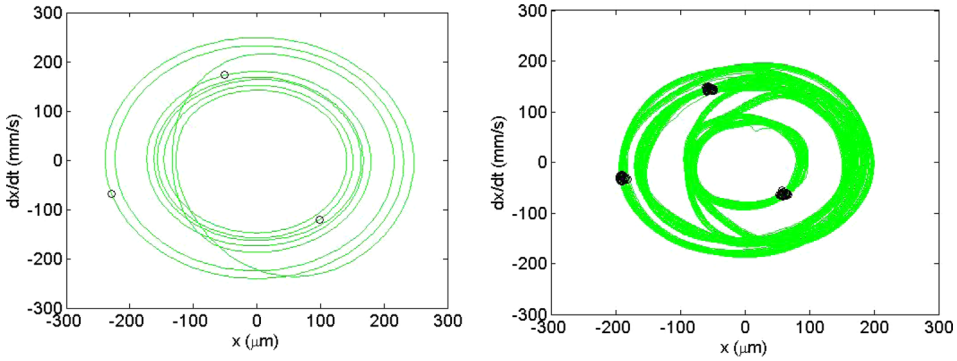

Fig. 10 Poincaré maps for 3800 rpm, 4.5 mm axial depth (left) simulated; (right) experiment

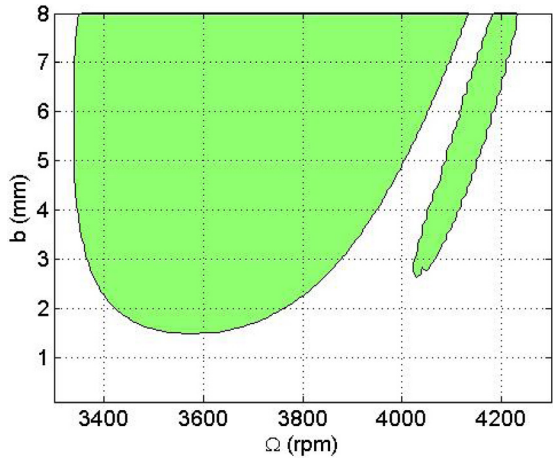

Fig. 11 Simulated stability map for experimental setup ($M = 1$ μm contour)

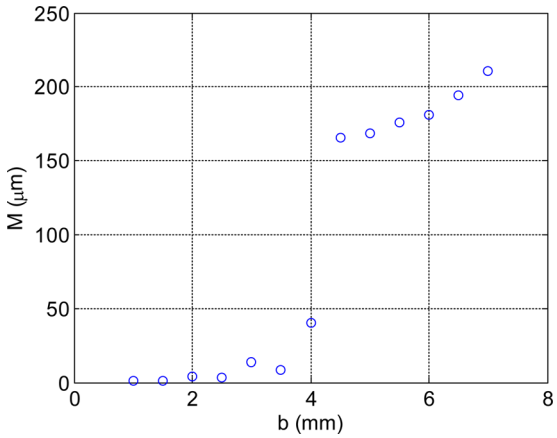

Fig. 12 *M* values for experiments (3800 rpm)

Poincaré maps for an axial depth of 4.5 mm. Good agreement is observed.

A simulated stability map for the same axial depth of cut range, but spindle speeds from 3300 rpm to 4300 rpm is displayed in Fig. 11. The spindle speed resolution is again 10 rpm, the axial depth resolution is 0.1 mm, and the initial transients were removed prior to analysis. The transition from stable to unstable behavior at 3800 rpm depicted in Fig. 9 is replicated.

Table 1 Numerical *M* values from experiments (3800 rpm)

b (mm)	M (μm)
1.0	1.0
1.5	0.8
2.0	4.3
2.5	3.6
3.0	13.3
3.5	8.6
4.0	40.5
4.5	165.8
5.0	168.6
5.5	176.2
6.0	181.1
6.5	194.1
7.0	210.9

Although the stability metric described here is intended for automated stability identification in time domain simulation, the M values calculated from experiments are also included. The M values are plotted in the top panel of Fig. 12 and mimic the behavior observed in Fig. 9 (65 once-per-tooth sampled points were used). The numerical values are provided in Table 1.

Conclusions

This paper presented a new stability metric for analysis of milling time domain simulation signals. The focus was establishing an automated approach for identifying stability of time domain simulation results. The metric is based on periodic sampling of milling signals. Stable cutting conditions exhibit forced vibrations only and the sampled points repeat over time, while unstable cuts do not repeat with each tooth passage. By calculating the normalized sum of the absolute values of the differences between sequentially sampled points, a metric is presented which identifies stable and unstable behavior. A primary benefit is that the numerical limit between the two behaviors is nominally zero. In practice, an arbitrarily small value is selected to account for numerical precision in simulation. Experimental results were presented to validate the time domain simulation.

References

[1] Arnold, R. N., 1946, "The Mechanism of Tool Vibration in the Cutting of Steel," Proc. Inst. Mech. Eng., **154**(1), pp. 261–284.
[2] Doi, S., and Kato, S., 1956, "Chatter Vibration of Lathe Tools," ASME, **78**, pp. 1127–1134.
[3] Tobias, S. A., and Fishwick, W., 1958, "The Chatter of Lathe Tools Under Orthogonal Cutting Conditions," ASME, **80**, pp. 1079–1088.
[4] Tlusty, J., and Polacek, M., 1963, "The Stability of Machine Tools Against Self-Excited Vibrations in Machining," Int. Res. Prod. Eng., **1**(1), pp. 465–474.
[5] Tobias, S. A., 1965, *Machine Tool Vibration*, Wiley, New York.
[6] Merritt, H. E., 1965, "Theory of Self-Excited Machine-Tool Chatter," ASME J. Eng. Ind., **87**(4), pp. 447–454.
[7] Tlusty, J., and Polacek, M., 1968, "Experience With Analysing Stability of Machine Tool Against Chatter," MTDR Conference, pp. 521–570.
[8] Shridar, R., Hohn, R. E., and Long, G. W., 1968, "A General Formulation of the Milling Process Equation," ASME J. Eng. Ind., **90**(2), pp. 317–324.
[9] Hohn, R. E., Shridar, R., and Long, G. W., 1968, "A Stability Algorithm for a Special Case of the Milling Process," ASME J. Eng. Ind., **90**(2), pp. 326–329.
[10] Shridar, R., Hohn, R. E., and Long, G. W., 1968, "A Stability Algorithm for the General Milling Process," ASME J. Eng. Ind., **90**(2), pp. 330–334.
[11] Hanna, N. H., and Tobias, S. A., 1974, "A Theory of Nonlinear Regenerative Chatter," J. Eng. Ind., **96**(1), pp. 247–255.
[12] Tlusty, J., and Ismail, F., 1981, "Basic Non-Linearity in Machining Chatter," Ann. CIRP, **30**(1), pp. 299–304.
[13] Tlusty, J., and Ismail, F., 1983, "Special Aspects of Chatter in Milling," ASME J. Vib., Stress Reliab. Des., **105**(1), pp. 24–32.
[14] Tlusty, J., 1985, "Machine Dynamics," *Handbook of High-Speed Machining Technology*, R. I. King, ed., Chapman and Hall, New York, pp. 48–153.
[15] Tlusty, J., 1986, "Dynamics of High-Speed Milling," ASME J. Eng. Ind., **108**(2), pp. 59–67.
[16] Minis, I., and Yanusevsky, R., 1993, "A New Theoretical Approach for Prediction of Chatter in Milling," ASME J. Eng. Ind., **115**(1), pp. 1–8.
[17] Altintas, Y., and Budak, E., 1995, "Analytical Prediction of Stability Lobes in Milling," Ann. CIRP, **44**(1), pp. 357–362.
[18] Davies, M. A., Dutterer, B. S., Pratt, J. R., and Schaut, A. J., 1998, "On the Dynamics of High-Speed Milling With Long, Slender Endmills," Ann. CIRP, **47**(1), pp. 55–60.
[19] Moon, F. C., and Kalmár-Nagy, T., 2001, "Nonlinear Models for Complex Dynamics in Cutting Materials," Philos. Trans. R. Soc. London A, **359**(1781), pp. 695–711.
[20] Davies, M. A., Pratt, J. R., Dutterer, B. S., and Burns, T. J., 2000, "The Stability of Low Radial Immersion Milling," Ann. CIRP, **49**(1), pp. 37–40.
[21] Moon, F. C., 1994, "Chaotic Dynamics and Fractals in Material Removal Processes," *Nonlinearity and Chaos in Engineering Dynamics*, J. Thompson, and S. Bishop, eds., Wiley, New York, pp. 25–37.
[22] Bukkapatnam, S., Lakhtakia, A., and Kumara, S., 1995, "Analysis of Senor Signals Shows Turning on a Lathe Exhibits Low-Dimensional Chaos," Phys. Rev. E, **52**(3), pp. 2375–2387.
[23] Stépán, G., and Kalmár-Nagy, T., 1997, "Nonlinear Regenerative Machine Tool Vibrations," ASME Paper No. DETC 97/VIB-4021.
[24] Nayfey, A., Chin, C., and Pratt, J., 1998, "Applications of Perturbation Methods to Tool Chatter Dynamics," *Dynamics and Chaos in Manufacturing Processes*, F. C. Moon, ed., Wiley, New York, pp. 193–213.
[25] Minis, I., and Berger, B. S., 1998, "Modelling, Analysis, and Characterization of Machining Dynamics," *Dynamics and Chaos in Manufacturing Processes*, F. C. Moon, ed., Wiley, New York, pp. 125–163.

[26] Moon, F. C., and Johnson, M., 1998, "Nonlinear Dynamics and Chaos in Manufacturing Processes," *Dynamics and Chaos in Manufacturing Processes*, F. C. Moon, ed., Wiley, New York, pp. 3–32.
[27] Smith, K. S., and Tlusty, J., 1991, "An Overview of Modeling and Simulation of the Milling Process," J. Eng. Ind., **113**(2), pp. 169–175.
[28] Campomanes, M. L., and Altintas, Y., 2003, "An Improved Time Domain Simulation for Dynamic Milling at Small Radial Immersions," ASME J. Manuf. Sci. Eng., **125**(3), pp. 416–422.
[29] Zhao, M. X., and Balachandran, B., 2001, "Dynamics and Stability of Milling Process," Int. J. Solids Struct., **38**, pp. 2233–2248.
[30] Davies, M. A., Pratt, J. R., Dutterer, B., and Burns, T. J., 2002, "Stability Prediction for Low Radial Immersion Milling," ASME J. Manuf. Sci. Eng., **124**(2), pp. 217–225.
[31] Mann, B. P., Insperger, T., Bayly, P. V., and Stépán, G., 2003, "Stability of Up-Milling and Down-Milling, Part 2: Experimental Verification," Int. J. Mach. Tools Manuf., **43**(1), pp. 35–40.
[32] Mann, B. P., Insperger, T., Bayly, P. V., and Stépán, G., 2003, "Stability of Up-Milling and Down-Milling, Part 1: Alternative Analytical Methods," Int. J. Mach. Tools Manuf., **43**(1), pp. 25–34.
[33] Insperger, T., Stépán, G., Bayly, P. V., and Mann, B. P., 2003, "Multiple Chatter Frequencies in Milling Processes," J. Sound Vib., **262**(2), pp. 333–345.
[34] Insperger, T., and Stépán, G., 2004, "Vibration Frequencies in High-Speed Milling Processes or a Positive Answer to Davies, Pratt, Dutterer, and Burns," ASME J. Manuf. Sci. Eng., **126**(3), pp. 481–487.
[35] Mann, B. P., Bayly, P. V., Davies, M. A., and Halley, J. E., 2004, "Limit Cycles, Bifurcations, and Accuracy of the Milling Process," J. Sound Vib., **277**, pp. 31–48.
[36] Merdol, S. D., and Altintas, Y., 2004, "Multi Frequency Solution of Chatter Stability for Low Immersion Milling," ASME J. Manuf. Sci. Eng., **126**(3), pp. 459–466.
[37] Govekar, E., Gradišek, J., Kalveram, M., Insperger, T., Weinert, K., Stepan, G., and Grabec, I., 2005, "On Stability and Dynamics of Milling at Small Radial Immersion," Ann. CIRP, **54**(1), pp. 357–362.
[38] Gradišek, J., Kalveram, M., Insperger, T., Weinert, K., Stépán, G., Govekar, E., and Grabec, I., 2005, "On Stability Prediction for Milling," Int. J. Mach. Tools Manuf., **45**(7–8), pp. 769–781.
[39] Mann, B. P., Garg, N. K., Young, K. A., and Helvey, A. M., 2005, "Milling Bifurcations From Structural Asymmetry and Nonlinear Regeneration," Nonlinear Dyn., **42**(4), pp. 319–337.
[40] Stépán, G., Szalai, R., Mann, B. P., Bayly, P. V., Insperger, T., Gradisek, J., and Govekar, E., 2005, "Nonlinear Dynamics of High-Speed Milling—Analyses, Numerics, and Experiments," ASME J. Vib. Acoust., **127**(2), pp. 197–203.
[41] Zatarain, M., Muñoa, J., Peigné, G., and Insperger, T., 2006, "Analysis of the Influence of Mill Helix Angle on Chatter Stability," Ann. CIRP, **55**(1), pp. 365–368.
[42] Insperger, T., Munoa, J., Zatarain, M. A., and Peigné, G., 2006, "Unstable Islands in the Stability Chart of Milling Processes Due to the Helix Angle," CIRP 2nd International Conference on High Performance Cutting, Vancouver, Canada, June, pp. 12–13.
[43] Patel, B. R., Mann, B. P., and Young, K. A., 2008, "Uncharted Islands of Chatter Instability in Milling," Int. J. Mach. Tools Manuf., **48**(1), pp. 124–134.
[44] Schmitz, T., and Smith, K. S., 2009, *Machining Dynamics: Frequency Response to Improved Productivity*, Springer, New York.
[45] Schmitz, T., Davies, M., Medicus, K., and Snyder, J., 2001, "Improving High-Speed Machining Material Removal Rates by Rapid Dynamic Analysis," Ann. CIRP, **50**(1), pp. 263–268.
[46] Schmitz, T., Medicus, K., and Dutterer, B., 2002, "Exploring Once-Per-Revolution Audio Signal Variance as a Chatter Indicator," Mach. Sci. Technol., **6**(2), pp. 215–233.
[47] Schmitz, T., 2003, "Chatter Recognition by a Statistical Evaluation of the Synchronously Sampled Audio Signal," J. Sound Vib., **262**(3), pp. 721–730.